



Published in final edited form as:

*J Am Soc Mass Spectrom.* 2018 February ; 29(2): 316–322. doi:10.1007/s13361-017-1750-8.

## Towards High-Resolution Tissue Imaging Using Nanospray Desorption Electrospray Ionization Mass Spectrometry Coupled to Shear Force Microscopy

Son N. Nguyen<sup>a)</sup>, Ryan L. Sontag<sup>b)</sup>, James P. Carson<sup>c)</sup>, Richard A. Corley<sup>b)</sup>, Charles Ansong<sup>b)</sup>, and Julia Laskin<sup>a)</sup>\*

<sup>a)</sup>Physical Sciences Division, Pacific Northwest National Laboratory, Richland, WA, USA

<sup>b)</sup>Biological Sciences Division, Pacific Northwest National Laboratory, Richland, WA, USA

<sup>c)</sup>Texas Advanced Computing Center, University of Texas at Austin, Austin, TX 78758, USA

### Abstract

Constant mode ambient mass spectrometry imaging (MSI) of tissue sections with high lateral resolution of better than 10  $\mu\text{m}$  was performed by combining shear force microscopy with nanospray desorption electrospray ionization (nano-DESI). Shear force microscopy enabled precise control of the distance between the sample and nano-DESI probe during MSI experiments and provided information on sample topography. Proof-of-concept experiments were performed using lung and brain tissue sections representing spongy and dense tissues, respectively. Topography images obtained using shear force microscopy were comparable to the results obtained using contact profilometry over the same region of the tissue section. Variations in tissue height were found to be dependent on the tissue type and were in the range of 0–5  $\mu\text{m}$  for lung tissue and 0–3  $\mu\text{m}$  for brain tissue sections. Ion images of phospholipids obtained in this study are in good agreement with literature data. Normalization of nano-DESI MSI images to the signal of the internal standard added to the extraction solvent allowed us to construct high-resolution ion images free of matrix effects.

### Keywords

high-resolution imaging mass spectrometry; nanospray desorption electrospray ionization (nano-DESI); shear force microscopy; mouse lung tissue; phospholipids; metabolites

### Introduction

Ambient mass spectrometry imaging (MSI) enables spatial localization of molecules in biological systems in their native state.[1–3] Since the introduction of desorption electrospray ionization (DESI),[4] numerous ambient MSI techniques have been developed for biological research as described in recent reviews.[5–13] One class of ambient MSI techniques relies on localized liquid extraction of molecules from surfaces followed by soft

Author for correspondence: Julia Laskin (Julia.Laskin@pnnl.gov), Physical Sciences Division, Pacific Northwest National Laboratory, PO Box 999, K8-88, Richland, WA 99352 USA.

ionization.[14] These include DESI,[4, 15] easy ambient sonic spray ionization (EASI),[16] liquid microjunction surface sampling probe (LMJ-SSP),[17] nanospray desorption electrospray ionization (nano-DESI),[18] single probe,[19] liquid extraction surface sampling (LESA),[20] scanning probe electrospray ionization (SPESI),[21] and others. Advantages of liquid extraction ambient ionization techniques include reproducibility, high sensitivity, online derivatization, and quantification of extracted analyte molecules using appropriate standards in the working solvent.[14] For example, online quantification of drugs and their metabolites in imaging experiments has been performed by several groups by adding deuterated standards to the solvent.[22, 23] Furthermore, shotgun-like quantification of phospholipids has been demonstrated using nanospray desorption electrospray ionization mass spectrometry imaging (nano-DESI MSI).[24] A similar approach, in which the signal of the extracted analyte is normalized to the signal of the standard continuously supplied throughout the imaging experiment, has been used to compensate for matrix effects in MSI. [25]

One of the challenges associated with liquid extraction-based ambient MSI is that these techniques often require precise control of the distance between the sample and the extraction probe for robust and reproducible operation.[26–28] One notable exemption is DESI that can tolerate surface irregularities of the order of several microns. Several approaches have been developed to facilitate constant distance ambient imaging using liquid extraction techniques. For example, van Berkel and co-workers have developed an image analysis-based approach to control the distance between a liquid micro junction surface sampling probe (LMJ-SSP) and a sample surface.[27] In this approach, the shadow of the probe on the surface is continuously monitored using a CCD camera and the distance is adjusted using a custom image analysis software. In a commercially available version of the LMJ-SSP device, flowprobe (Prosolia Inc.), a laser distance sensor is used to control the height of the probe relative to the sample surface. This approach is well-suited for the analysis of reflective samples. A simple method was developed by our group for imaging of relatively uniform samples such as thin tissue sections on glass slides using nano-DESI MSI. [28] In this approach, it is assumed that variations in the sample height are minor and the distance between the sample and the probe is controlled by defining a plane, in which the sample resides.

Recently, we introduced a new technique for imaging samples of arbitrary topography by combining shear force microscopy with nano-DESI MSI.[26] Shear force microscopy enables imaging of sample topography by measuring a shear force between an oscillating finely-pulled nanopipette and a sample surface.[29] The distance between the sample and the shear force probe is continuously adjusted throughout the experiment to maintain the oscillation amplitude of a resonant mode most sensitive to the sample surface at a constant value.[30] By incorporating the shear force nanopipette into the nano-DESI probe, we were able to conduct constant-distance nano-DESI MSI of living microbial communities directly from agar plates.[26] In these experiments, the shear force probe allowed us to follow variations in sample height of up to 0.8 mm while acquiring mass spectral data with a moderate spatial resolution of ~200  $\mu\text{m}$ . Herein, we demonstrate that this approach enables imaging of thin tissue sections with high spatial resolution. Although high spatial resolution nano-DESI MSI has been previously demonstrated,[28] the initial experiments were

performed using brain tissue sections that do not exhibit substantial height variation. However, other types of tissues may have fairly rough topography, which necessitates the use of a shear force or another feedback mechanism for imaging these samples with high spatial resolution. Herein, we demonstrate that height variations in tissue sections are different for different types of tissues. Furthermore, this study establishes an approach for high-resolution nano-DESI MSI of tissue sections using shear force feedback mode to control the distance between the sample and nano-DESI probe.

## Experimental section

### Tissue collection and handling

Lung tissue samples were generated at the Cincinnati Children's Hospital Medical Center. The mice were housed in the Cincinnati Children's Hospital Medical Center Animal Care Facility according to National Institutes of Health and institutional guidelines for the use of laboratory animals. All experimental protocols were reviewed and approved by Cincinnati Children's Hospital Research Foundation Institutional Animal Care and Use Committee. C57BL/6 mice from JAX Mice (Jackson Laboratory, Bar Harbor, ME, USA) were sacrificed at day 7 by CO<sub>2</sub> overdose. Lungs were collected, cleaned, embedded in carboxy-methyl cellulose (CMC) and stored in -80°C freezer. CMC embedding medium was prepared using a literature procedure [31]. Briefly, 10 g of Sodium CMC (Catalog number 419273, Sigma, St. Louis) was added to 450 mL of deionized water pre-heated to 70 °C and incubated overnight at 70 °C with shaking. The mixture was subsequently brought to 500 mL by adding deionized water, thoroughly mixed, and refrigerated until use. For embedding, the lung was placed in a plastic mold filled with ice cold CMC on dry ice. Ice cold CMC was added as needed to cover the lung and the mold was stored at -80°C. Fresh frozen mouse brain tissue samples from 10 week-old C57BL/6 mice were provided by Dr. Jordan Smith from PNNL and stored at -80°C. For imaging experiments, samples were sectioned into 10 µm thick slices with a Thermo CryoStar NX70 (Thermo Scientific, Waltham, MA) microtome. Coronal sections of the lung and brain tissue were examined in this study. Sections were thaw-mounted onto regular glass slides and stored at -80°C until analysis. The section was allowed to thaw at room temperature right before mounting onto the nano-DESI sample holder for analysis.

### Nano-DESI imaging

A custom designed nano-DESI imaging source was mounted onto a linear ion trap (LTQ) Orbitrap mass spectrometer (LTQ-Orbitrap XL, Thermo Scientific, Bremen, Germany) operated in a positive mode with a mass resolution of 60,000 ( $m/m$  at  $m/z$  400). The nano-DESI probe was assembled using two fused silica capillaries (50 × 150 µm, ID × OD, Polymicro Technologies) finely pulled to ~10 µm. A third pulled capillary (200 × 800 µm, ID × OD) with a 20 µm OD tip served as a shear force probe. The capillary was pulled using a laser-based micropipette puller system (P-2000, Sutter Instrument, Novato, CA). Two 3 × 3 × 0.55 mm 3.8 MHz piezoelectric ceramic plates (Steiner & Martins, Inc. Doral, FL) were attached to the shear force probe. The top plate induced low-amplitude vibration of the nano-DESI probe using a sinusoidal waveform generated by a function generator (Agilent 33220A, Agilent Technologies, Santa Clara, CA). The second piezoelectric plate positioned

closer to the sample surface was used to detect the tip oscillation amplitude through a lock-in amplifier (Model SR865, Stanford Research Systems, Sunnyvale, CA) that operates in a range of frequencies of 1 mHz–2 MHz.

Each capillary was independently positioned using a high-precision micromanipulator (XYZ 500 MIM, Quarter Research, Bend, Oregon). The relative position of the capillaries with respect to each other and the mass spectrometer inlet was visualized using two Dino-Lite digital microscopes (AnMo Electronics Corporation, Sanchong, New Taipei, Taiwan). A microscope glass slide containing tissue sections was placed in a custom-designed nano-DESI sample holder attached to a motorized XYZ stage (Zaber Technologies, Vancouver, Canada). The sample position was controlled using a custom-designed LabVIEW software described in our previous study.[28] A 9:1 methanol:water mixture containing 0.5  $\mu\text{M}$  concentration of 1-nonadecanoyl-2-hydroxy-sn-glycero-3-phosphocholine (LPC 19:0, Avanti Polar Lipids, Alabaster, Alabama) was used as a working solvent. The solvent was delivered via a syringe pump (Legato 180, KD Scientific) through the primary capillary to the sample at a flow rate of 0.3  $\mu\text{l}/\text{min}$ . Ions were produced by electrospray ionization from the secondary capillary at the mass spectrometer inlet by applying a high voltage of 3.0 kV to the syringe needle. The heated capillary was kept at 250°C.

Imaging experiments were performed by scanning the sample under the shear force nano-DESI probe in lines at a constant velocity of 5  $\mu\text{m}/\text{s}$  while acquiring high-resolution mass spectra at a rate of 1.2 spectrum/s. The lines were spaced by 10  $\mu\text{m}$ . As a result, the pixel size in these experiments was 4 $\mu\text{m}$  x 10 $\mu\text{m}$ . We note that the pixel size may not be directly correlated to the spatial resolution, which depends on the size of the liquid bridge in contact with the sample and possible diffusional broadening during analysis. The spatial resolution obtained in these experiments will be discussed later in the text. Incorporation of the shear force probe allowed us to control the distance between the sample and the nano-DESI probe on the fly by adjusting the z-position of the sample according to the feedback received from the shear force measurement. The feedback is obtained by measuring the amplitude of lateral oscillations of the shear force probe at a selected resonant frequency affected by shear forces between the sample and the tip of the shear force probe. Prior to each imaging experiment, the characteristic oscillation frequencies of the shear force probe sensitive to the sample were determined by acquiring probe excitation spectra in air and on the sample surface. It was found that signal amplitude at 128 KHz was most sensitive to the surface. In the next experiment, an approach curve was acquired by fixing the excitation frequency at 128 KHz and measuring the oscillation amplitude at this frequency as a function of the probe-to-surface distance. Finally, the probe-to-surface distance was fixed by setting the voltage measured by the detection piezo at 80% of its value in air. The value of the voltage was maintained throughout the imaging experiment by adjusting the sample-to-probe distance using a closed-loop feedback system controlled by the Labview program. Topographic data for each line scan were saved in individual data files. Topography images were constructed and baseline corrected using Origin Pro 2015 (Origin Lab, Northampton, MA). Baseline correction procedure is illustrated in Figure S1 of the supporting information. Ion images were generated using the customized imaging software, MSI QuickView, developed at Pacific Northwest National Laboratory.[32] All ion images were normalized to the sodium adduct of the LPC 19:0 standard at  $m/z$  560.3688.

## Results and discussion

Figure 1A shows an optical image of a representative mouse lung tissue section used in this study and Figure 1B shows a close up of a small part of the tissue section containing an airway imaged with high spatial resolution. High spatial resolution was achieved using a combination of shear force microscopy with nano-DESI MSI,[26] which enabled simultaneous imaging of sample topography and chemical composition. Figure 1C depicts a topography image of this part of the tissue section showing variations in the sample height of up to 6  $\mu\text{m}$  around the airway. As previously detailed, topography and ion images were acquired by scanning the sample under the probe at 5  $\mu\text{m}/\text{s}$ . At higher scanning velocities, we observed substantial vibrations of the sample holder, which obscured sample topography. Even at the slow scan rate used in this study, vibrations of the sample holder were clearly visible in the raw topography data shown in Figure S1 of the supporting information. Manual background subtraction from the measured topography data described in the supporting information was performed to generate the image shown in Figure 1C. An overlay of the optical and topography images shown in Figure 1D confirms good overlap between the elevated features in the tissue section observed using shear force microscopy and the airway boundary clearly seen using optical microscopy.

Figure 2 shows selected ion images acquired over the tissue section using a high-resolution nano-DESI probe described in detail in the experimental section. Previously, Murphy and co-authors presented a detailed study of the phospholipid distributions in adult mouse lung tissue using matrix-assisted laser desorption ionization (MALDI) MSI.[33] They observed that phospholipids containing polyunsaturated arachidonic (FA 20:4) and docosahexaenoic (FA 22:6) acids, PC 16:0/20:4 and PC 16:0/22:6, were localized at the airway linings. The enhanced abundance of polyunsaturated fatty acids along the airways emphasizes the important role of these species as precursors to prostaglandins and lipid mediators that are implicated in several pulmonary diseases. Ion images depicted in Figure 2 provide additional support for this assertion. Specifically, we observe tight localization of polyunsaturated LPC, LPE, and PC species including LPC 20:4, LPE 22:6, PC 36:4, and PC 38:6 along the airway. In addition, Murphy and co-authors proposed that phospholipids containing polyunsaturated fatty acid tail groups originate from pulmonary cellular membranes.[33] This conclusion is based on the tight localization of these species along the airways and their low concentrations in pulmonary surfactant. Detailed lipidomics characterization of adult mouse lung tissue revealed elevated levels of long chain polyunsaturated fatty acids and LPC species in adult mice in comparison with pups.[34] This observation was attributed to a greater state of inflammation of adult lungs maintained in a healthy state through a fine balance between pro-inflammatory and pro-resolution lipids and associated protein mediators.

In contrast, more saturated phospholipids indicate uniform alveolar localization in their distribution. Ion images of PC 32:0 ( $m/z$  734.5700) and PC 34:1 ( $m/z$  760.5856) obtained in this study are consistent with the results of Murphy and co-authors.[33] Specifically, MALDI images of PC 16:0/16:0 and PC 16:0/18:1 obtained in that study indicated uniform distribution of these species in the lung parenchyma. PC 16:0/16:0 is known to be essential for the pulmonary surfactant function[35] and, as such, is conserved across animal species. [36] PC 16:0/16:0 accounts for approximately 40% of the total phospholipid content of

mammalian surfactant with the remaining fraction composed of singly and di-unsaturated PC species and a small amount of other types of phospholipids.[35] The alveolar localization of PC 16:0/16:0 and PC 16:0/18:1 is consistent with their important role in lung surfactant. Interestingly, the spatial localization of LPC 18:1 is different from the distribution obtained for alveolar PC species, PC 32:0 and PC 34:1. Specifically, this phospholipid is found both in the alveolar region of the tissue and along the airway. Similar spatial localization was observed for LPC 16:0, LPC 18:0, and LPC 18:2. The inflammatory activity of these LPC species in lungs have been previously investigated.[37] It has been demonstrated that bronchial epithelial cells release LPC 16:0, LPC 18:0, and LPC 18:1 in response to vascular endothelial growth factor stimulation and that the release of these LPC species may induce inflammatory injury of airway epithelium. Our results indicate that LPC 16:0, LPC 18:0, and LPC 18:2 may play a role both as components of lung surfactant and pro-inflammatory species in the biology of healthy lungs. In addition, other abundant PC species including LPC 16:0, LPC 18:2, LPC 18:0, LPC 16:0, PC 30:0, PC 32:1, PC 34:2, PC 38:5, PC 38:4, and PC 40:6 were observed in nano-DESI MSI data. In our recent lipidomics study, these PC species have been also observed as abundant components of lung tissue.[34]

The observed variation in the topography of the lung tissue section (Figure 1C) highlights the importance of shear force microscopy as a feedback mechanism for high spatial resolution nano-DESI MSI experiments. In particular, we estimate that a precisely controlled distance between the sample and the high-resolution nano-DESI probe of  $\sim 1 \mu\text{m}$  should be maintained in order to achieve a spatial resolution of better than  $10 \mu\text{m}$ . The brittle spongy nature of lung tissue poses unique challenges both to the sample preparation protocols and imaging methodology. In order to better understand challenges associated with imaging of other types of tissues, we examined the morphology of a  $10 \mu\text{m}$  thin brain tissue section on a glass slide. Brain tissue is very dense and represents another extreme, at which the ability to precisely control the height of the sample in the imaging experiment may be less important in comparison with lung tissue. The topography of a small portion of a coronal mouse brain tissue section (Figure 3A) acquired using contact profilometry and shear force microscopy is shown in Figures 3D and 3E, respectively. The difference between the results obtained using these two techniques is attributed to vibrations of the sample holder during shear force microscopy measurement. Of note is the fact that shear force measurement was performed in conjunction with nano-DESI MSI on a sample mounted in front of a mass spectrometer. In this configuration, it is difficult to eliminate vibrations of the sample holder, which contributes to periodic noise observed in our shear force images. Nevertheless, the correspondence between topography images shown in Figures 3D and 3E is quite good and indicates that, despite this complication, shear force measurement provides reliable results.

Topography images (Figures 3D and 3E) indicate height variations of less than  $3 \mu\text{m}$  across the brain tissue section, which is smaller in comparison with lung tissue shown in Figure 1C. Nevertheless, obvious changes in topography that may affect the results of high-resolution nano-DESI MSI are clearly seen in the image. By comparing our results with mouse brain atlas annotations (Figures 3B and C), it is possible to correlate the observed topography to the anatomical features of the mouse brain. Specifically, the lack of tissue observed in the region corresponding to the third ventricle (2) is consistent with its fluid-filled nature. Meanwhile, the highest elevation of  $\sim 3 \mu\text{m}$  is observed in the alveus (5) and isocortex (9). In



addition, a scratch originating from tissue sectioning is clearly observed as a  $\sim 3 \mu\text{m}$  tall feature in the topography image. The next high-elevation regions of  $1.5\text{--}2.5 \mu\text{m}$  correspond to corpus callosum (3) and subiculum (6); other regions of the brain tissue highlighted in Figure 3C have an average elevation of  $\sim 1 \mu\text{m}$ . These observations indicate that although less pronounced height variations may be present in more dense tissues such as brain, they should still be taken into consideration when performing imaging experiments with high spatial resolution.

Selected ion images acquired along with the shear force image of the brain tissue are shown in Figure 3F. A complete set of ion images is shown in Table S1 of the supporting information. The species were identified based on the accurate mass, MS/MS data, and comparison with literature. Ion images shown in Figure 3F correspond to sodium adducts of LPC 16:0 at  $m/z$  518.3232, PE(O-36:3) or PE(P-36:2) at  $m/z$  750.5418, SM (d36:1) at  $m/z$  753.5902, PC 32:1 at  $m/z$  754.5381, PE 38:4 at  $m/z$  790.5372, and SM (d42:2) at  $m/z$  835.6676. Aside from similar distributions of LPC 16:0 and SM (d36:1) enhanced in the gray matter, distinctly different images were obtained for different types of phospholipids. For example, plasmalogen PE species at  $m/z$  750.5418 is tightly localized to the white matter regions 3 (corpus callosum) and 5 (alveus). This phospholipid is observed at lower abundance in the dorsal hippocampal commissure (4) and lines up the boundary of the dentate gyrus. Although SM (d42:2) at  $m/z$  835.6676 is also localized to the white matter, substantial abundance of this species is also observed in the cortex. The observed localization of SM (d42:2) in the white matter and a distinctly different distribution of SM (d36:1) at  $m/z$  753.5902 preferentially localized in the gray matter is consistent with the literature data.[38] Sphingomyelins are tightly regulated in the brain by sphingomyelin synthase. Recent study demonstrated that at least two isoforms of sphingomyelin synthase are differentially expressed in different types of neuronal cells.[39] Different localization of sphingomyelins observed in this study could be an indication of their synthesis by different sphingomyelin synthase isoforms.

Although both PC 32:1 at  $m/z$  754.5381 and PE 38:4 at  $m/z$  790.5372 are distributed fairly uniformly in the tissue, some differences are observed in the localization of these phospholipids. Specifically, PC 32:1 is clearly suppressed in the dorsal hippocampal commissure (4) and subiculum (6). These minor changes in the phospholipid distribution can be observed using high spatial resolution imaging enabled through the combination of shear force microscopy and nano-DESI MSI described in this study. Regional selectivity of different brain regions to PC species with specific number of double bonds has been previously observed in nano-DESI MSI experiments, in which shotgun-like quantification of abundant PC species was performed by adding two internal standards to the extraction solvent. It has been demonstrated that by normalizing signals of endogenous lipids to the abundance of the standard in each pixel efficiently compensates for signal suppression in imaging experiments.[25] A similar approach was used in this study to produce ion images free of matrix effects but with much higher spatial resolution that helps reveal interesting variations in phospholipids concentrations in tissues. In summary, the combination of shear force microscopy with nano-DESI MSI enables quantitative imaging of lipids and metabolites in thin tissue sections with high spatial resolution. The upper limit estimate of the spatial resolution achieved in this study is  $10 \mu\text{m}$ . The spatial resolution in these

experiments is determined by the size of the capillaries comprising the nano-DESI probe and limited by the sensitivity of a mass spectrometer crucial to detection of increasingly low signals from small extraction volumes analyzed at higher resolution. The experimental approach presented in this study will enable ambient imaging of tissue sections with a spatial resolution approaching some of the best results obtained using matrix assisted laser desorption ionization (MALDI).[40–42]

## Conclusions

In this study, we demonstrated for the first time the utility of nano-DESI MSI combined with shear force microscopy for high-resolution imaging of tissue sections. This approach enables simultaneous imaging of topography and chemical gradients of numerous molecules in tissue sections. Both spongy mouse lung and dense mouse brain tissues were examined in this study to explore a range of height variations across a typical tissue sample examined in ambient imaging experiments. It is demonstrated that despite the interference of vibrations originating from a mass spectrometer, topography images obtained using shear force microscopy during nano-DESI MSI experiments are consistent with topography images obtained using an established contact profilometry technique. Vibrations of the surface holder become particularly severe at higher scan rates ( $>5 \mu\text{m/s}$  in our experimental setup). Nevertheless, even in the presence of vibrations, the shear force probe provides adequate control of the distance between the sample and the nano-DESI probe, which is important for imaging experiments. Ion images obtained in our proof-of-concept experiments are consistent with literature results. The approach presented in this study is not limited to nano-DESI MSI. A similar experimental setup can be adopted for mass spectrometry imaging of tissue sections using other types of proximity probes.[13]

## Supplementary Material

Refer to Web version on PubMed Central for supplementary material.

## Acknowledgments

The research described in this paper was supported by grant U01 HL122703 from the National Heart Lung Blood Institute of NIH and grant ES024229-01 from the National Institute of Environmental Health Sciences (NIEHS). We thank the LungMAP MouseHub (U01 HL122642) for provision of lung samples and Rosey Chu (PNNL) for help with preparation of the CMC embedding medium. The research was performed at EMSL, a national scientific user facility sponsored by the DOE's Office of Biological and Environmental Research and located at Pacific Northwest National Laboratory (PNNL) in Richland, WA. PNNL is a multi-program national laboratory operated by Battelle for the DOE under contract DE-AC05-76RLO 1830.

## References

1. Wu C, Dill AL, Eberlin LS, Cooks RG, Ifa DR. Mass spectrometry imaging under ambient conditions. *Mass Spectrom Rev.* 2013; 32:218–243. [PubMed: 22996621]
2. Nemes P, Vertes A. Ambient mass spectrometry for in vivo local analysis and in situ molecular tissue imaging. *TrAC, Trends Anal Chem.* 2012; 34:22–34.
3. Cooks RG, Ouyang Z, Takats Z, Wiseman JM. Ambient mass spectrometry. *Science.* 2006; 311:1566–1570. [PubMed: 16543450]



4. Takats Z, Wiseman JM, Gologan B, Cooks RG. Mass spectrometry sampling under ambient conditions with desorption electrospray ionization. *Science*. 2004; 306:471–473. [PubMed: 15486296]
5. Van Berkel GJ, Pasilis SP, Ovchinnikova O. Established and emerging atmospheric pressure surface sampling/ionization techniques for mass spectrometry. *J Mass Spectrom*. 2008; 43:1161–1180. [PubMed: 18671242]
6. Chen HW, Gamez G, Zenobi R. What Can We Learn from Ambient Ionization Techniques? *J Am Soc Mass Spectrom*. 2009; 20:1947–1963. [PubMed: 19748284]
7. Weston DJ. Ambient ionization mass spectrometry: current understanding of mechanistic theory; analytical performance and application areas. *Analyst*. 2010; 135:661–668. [PubMed: 20309440]
8. Greer T, Sturm R, Li LJ. Mass spectrometry imaging for drugs and metabolites. *Journal of Proteomics*. 2011; 74:2617–2631. [PubMed: 21515430]
9. Harris GA, Galhena AS, Fernandez FM. Ambient Sampling/Ionization Mass Spectrometry: Applications and Current Trends. *Anal Chem*. 2011; 83:4508–4538. [PubMed: 21495690]
10. Badu-Tawiah, AK., Eberlin, LS., Ouyang, Z., Cooks, RG. Chemical Aspects of the Extractive Methods of Ambient Ionization Mass Spectrometry. Johnson, MA., Martinez, TJ., editors. 2013.
11. Ellis SR, Brown SH, Panhuis MIH, Blanksby SJ, Mitchell TW. Surface analysis of lipids by mass spectrometry: More than just imaging. *Prog Lipid Res*. 2013; 52:329–353. [PubMed: 23623802]
12. Venter A, Nefliu M, Cooks RG. Ambient desorption ionization mass spectrometry. *Trac-Trends Anal Chem*. 2008; 27:284–290.
13. Venter AR, Douglass KA, Shelley JT, Hasman G, Honarvar E. Mechanisms of Real-Time, Proximal Sample Processing during Ambient Ionization Mass Spectrometry. *Anal Chem*. 2014; 86:233–249. [PubMed: 24308499]
14. Laskin J, Lanekoff I. Ambient Mass Spectrometry Imaging Using Direct Liquid Extraction Techniques. *Anal Chem*. 2016; 88:52–73. [PubMed: 26566087]
15. Takáts Z, Wiseman JM, Cooks RG. Ambient mass spectrometry using desorption electrospray ionization (DESI): instrumentation, mechanisms and applications in forensics, chemistry, and biology. *J Mass Spectrom*. 2005; 40:1261–1275. [PubMed: 16237663]
16. Haddad R, Sparrapan R, Kotiaho T, Eberlin MN. Easy Ambient Sonic-Spray Ionization-Membrane Interface Mass Spectrometry for Direct Analysis of Solution Constituents. *Anal Chem*. 2008; 80:898–903. [PubMed: 18179250]
17. Van Berkel GJ, Sanchez AD, Quirke JME. Thin-Layer Chromatography and Electrospray Mass Spectrometry Coupled Using a Surface Sampling Probe. *Anal Chem*. 2002; 74:6216–6223. [PubMed: 12510741]
18. Roach PJ, Laskin J, Laskin A. Nanospray desorption electrospray ionization: an ambient method for liquid-extraction surface sampling in mass spectrometry. *Analyst*. 2010; 135:2233–2236. [PubMed: 20593081]
19. Pan N, Rao W, Kothapalli NR, Liu R, Burgett AWG, Yang Z. The Single-Probe: A Miniaturized Multifunctional Device for Single Cell Mass Spectrometry Analysis. *Anal Chem*. 2014; 86:9376–9380. [PubMed: 25222919]
20. Kertesz V, Van Berkel GJ. Fully automated liquid extraction-based surface sampling and ionization using a chip-based robotic nanoelectrospray platform. *J Mass Spectrom*. 2010; 45:252–260. [PubMed: 20020414]
21. Otsuka Y, Shide S, Naito J, Kyogaku M, Hashimoto H, Arakawa R. Scanning probe electrospray ionization for ambient mass spectrometry. *Rapid Commun Mass Spectrom*. 2012; 26:2725–2732. [PubMed: 23124662]
22. Lanekoff I, Thomas M, Carson JP, Smith JN, Timchalk C, Laskin J. Imaging Nicotine in Rat Brain Tissue by Use of Nanospray Desorption Electrospray Ionization Mass Spectrometry. *Anal Chem*. 2013; 85:882–889. [PubMed: 23256596]
23. Parson WB, Koeniger SL, Johnson RW, Erickson J, Tian Y, Stedman C, Schwartz A, Tarcsa E, Cole R, Van Berkel GJ. Analysis of chloroquine and metabolites directly from whole-body animal tissue sections by liquid extraction surface analysis (LESA) and tandem mass spectrometry. *J Mass Spectrom*. 2012; 47:1420–1428. [PubMed: 23147817]

24. Lanekoff I, Thomas M, Laskin J. Shotgun Approach for Quantitative Imaging of Phospholipids Using Nanospray Desorption Electrospray Ionization Mass Spectrometry. *Anal Chem.* 2014; 86:1872–1880. [PubMed: 24428785]
25. Lanekoff I, Stevens SL, Stenzel-Poore MP, Laskin J. Matrix effects in biological mass spectrometry imaging: identification and compensation. *Analyst.* 2014; 139:3528–3532. [PubMed: 24802717]
26. Nguyen SN, Liyu AV, Chu RK, Anderton CR, Laskin J. Constant-Distance Mode Nanospray Desorption Electrospray Ionization Mass Spectrometry Imaging of Biological Samples with Complex Topography. *Anal Chem.* 2017; 89:1131–1137. [PubMed: 27973782]
27. Kertesz V, Ford MJ, Van Berkel GJ. Automation of a Surface Sampling Probe/Electrospray Mass Spectrometry System. *Anal Chem.* 2005; 77:7183–7189. [PubMed: 16285664]
28. Lanekoff I, Heath BS, Liyu A, Thomas M, Carson JP, Laskin J. Automated Platform for High-Resolution Tissue Imaging Using Nanospray Desorption Electrospray Ionization Mass Spectrometry. *Anal Chem.* 2012; 84:8351–8356. [PubMed: 22954319]
29. Brunner R, Bietsch A, Hollricher O, Marti O. Distance control in near-field optical microscopy with piezoelectrical shear-force detection suitable for imaging in liquids. *Rev Sci Instrum.* 1997; 68:1769–1772.
30. Ballesteros Katemann B, Schulte A, Schuhmann W. Constant-Distance Mode Scanning Electrochemical Microscopy (SECM)—Part I: Adaptation of a Non-Optical Shear-Force-Based Positioning Mode for SECM Tips. *Chemistry – A European Journal.* 2003; 9:2025–2033.
31. Stoeckli M, Staab D, Schweitzer A. Compound and metabolite distribution measured by MALDI mass spectrometric imaging in whole-body tissue sections. *Int J Mass Spectrom.* 2007; 260:195–202.
32. Thomas, M., Heath, BS., Laskin, J., Li, D., Liu, E., Hui, K., Kuprat, AP., van Dam, KK., Carson, JP. Visualization of High Resolution Spatial Mass Spectrometric Data during Acquisition. IEEE International Conference of the Engineering in Medicine and Biology Society (EMBS); 2012. p. 5545-5548.
33. Berry KAZ, Li BL, Reynolds SD, Barkley RM, Gijon MA, Hankin JA, Henson PM, Murphy RC. MALDI imaging MS of phospholipids in the mouse lung. *J Lipid Res.* 2011; 52:1551–1560. [PubMed: 21508254]
34. Dautel SE, Kyle JE, Clair G, Sontag RL, Weitz KK, Shukla AK, Nguyen SN, Kim YM, Zink EM, Luders T, Frevert CW, Gharib SA, Laskin J, Carson JP, Metz TO, Corley RA, Ansong C. Lipidomics reveals dramatic lipid compositional changes in the maturing postnatal lung. *Sci Rep-Uk.* 2017; 7
35. Veldhuizen R, Nag K, Orgeig S, Possmayer F. The role of lipids in pulmonary surfactant. *Biochimica et Biophysica Acta (BBA) - Molecular Basis of Disease.* 1998; 1408:90–108. [PubMed: 9813256]
36. Postle AD, Heeley EL, Wilton DC. A comparison of the molecular species compositions of mammalian lung surfactant phospholipids. *Comparative Biochemistry and Physiology Part A: Molecular & Integrative Physiology.* 2001; 129:65–73.
37. Zhuge Y, Yuan Y, van Breemen R, DeGrand M, Holian O, Yoder M, Lum H. Stimulated Bronchial Epithelial Cells Release Bioactive Lysophosphatidylcholine 16:0, 18:0, and 18:1. *Allergy Asthma Immunol Res.* 2014; 6:66–74. [PubMed: 24404396]
38. Martínez-Gardeazabal J, González de San Román E, Moreno-Rodríguez M, Llorente-Ovejero A, Manuel I, Rodríguez-Puertas R. Lipid mapping of the rat brain for models of disease. *Biochimica et Biophysica Acta (BBA) - Biomembranes.*
39. Kidani Y, Ohshima K-i, Sakai H, Kohno T, Baba A, Hattori M. Differential localization of sphingomyelin synthase isoforms in neurons regulates sphingomyelin cluster formation. *Biochem Biophys Res Commun.* 2012; 417:1014–1017. [PubMed: 22209789]
40. Römpf A, Guenther S, Schober Y, Schulz O, Takats Z, Kummer W, Spengler B. Histology by Mass Spectrometry: Label-Free Tissue Characterization Obtained from High-Accuracy Bioanalytical Imaging. *Angew Chem Int Ed.* 2010; 49:3834–3838.
41. Römpf A, Spengler B. Mass spectrometry imaging with high resolution in mass and space. *Histochemistry and Cell Biology.* 2013; 139:759–783. [PubMed: 23652571]

42. Chaurand P, Schriver KE, Caprioli RM. Instrument design and characterization for high resolution MALDI-MS imaging of tissue sections. *J Mass Spectrom.* 2007; 42:476–489. [PubMed: 17328093]

Author Manuscript

Author Manuscript

Author Manuscript

Author Manuscript

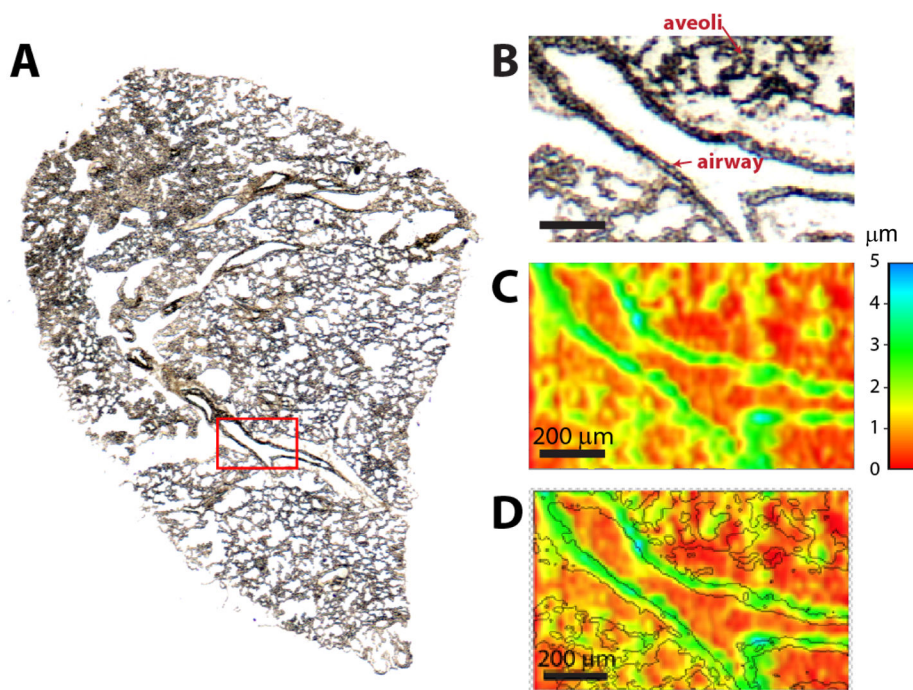


**Figure 1.** (A) Optical image of the lung tissue section highlighting a small,  $1 \times 0.5$  mm, region examined in this study. (B) Optical and (C) topography images of the region of the lung tissue selected for high-resolution nano-DESI MSI. (D) Overlay of the optical and topography images demonstrating overlap of the elevated parts of the tissue section with the airway.

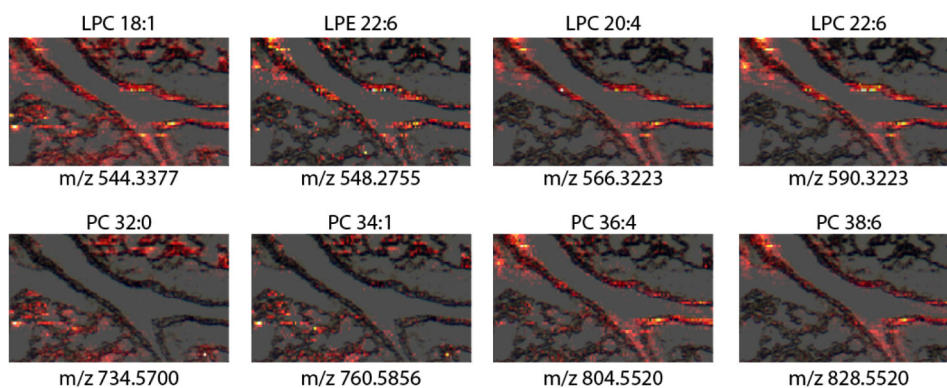


**Figure 2.** Ion images depicting the distribution of sodium adducts of LPC 18:1 (m/z 544.3377), LPE 22:6 (m/z 548.2755), LPC 20:4 (m/z 566.3223), LPC 22:6 (m/z 590.3223), PC 32:0 (m/z 734.5700), PC 34:1 (m/z 760.5856), PC 36:4 (m/z 804.5520), PC 38:6 (m/z 828.5520) overlaid on top of the optical image.

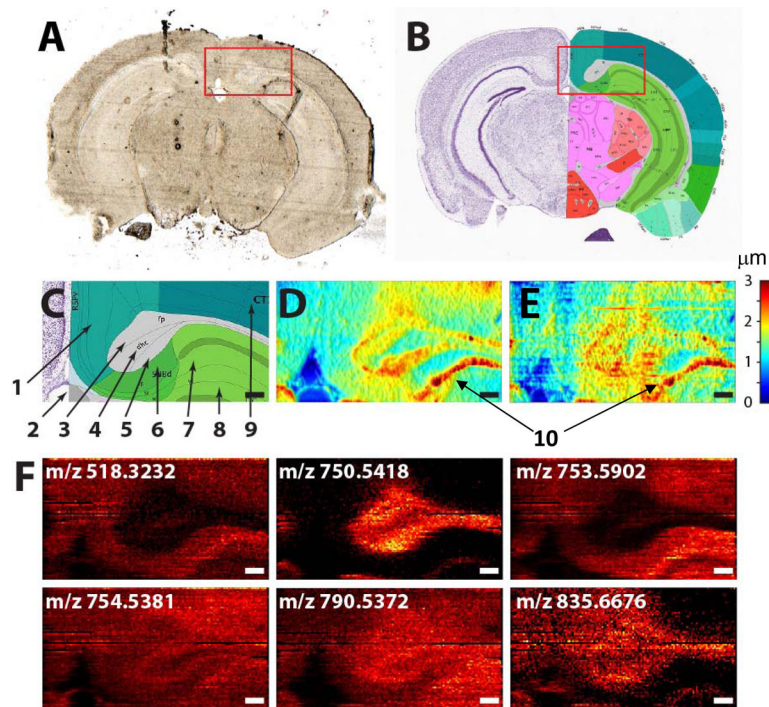


**Figure 3.** (A) Optical image of a coronal mouse brain tissue section and (B) a corresponding coronal section (#81) from the mouse brain atlas (<http://atlas.brain-map.org>); C) zoomed-in region corresponding to the red box in panel B with the following regions labeled: 1- retrosplenial cortex, 2-ventricle, 3-corpus callosum, 4-dorsal hippocampal commissure, 5- alveus, 6-subiculum, 7- hippocampal region CA1, 8-dentate gyrus, and 9-visual areas of isocortex. This area was analyzed using D) contact profilometry and E) topography image obtained using shear force microscopy. 10- a scratch observed in topography images. Color bar shows height in microns. F) Selected ion images obtained using nano-DESI MSI coupled to shear force microscopy. Scale bar is 200  $\mu\text{m}$ .